



# BER and channel capacity analysis of wireless system over $\kappa - \mu$ /inverse gamma and $\eta - \mu$ /inverse gamma composite fading model

Diwaker Pant<sup>1</sup> · Puspraj Singh Chauhan<sup>2</sup> · Sanjay Kumar Soni<sup>2</sup> · Sanjeev Naithani<sup>3</sup>

Accepted: 18 November 2020 / Published online: 2 January 2021  
© Springer Science+Business Media, LLC, part of Springer Nature 2021

## Abstract

The  $\kappa - \mu$ /Inverse Gamma (KMIG) and  $\eta - \mu$ /Inverse Gamma (EMIG) are recently introduced composite fading distributions for the precise design of the wireless systems, where multipath fading and shadowing occur concomitantly. Further, these composite fading models are competent to be employed in the performance investigation of the digital communication system as their mathematical formulations are quite tractable. Average symbol error probability (SEP) and channel capacity analysis are important parameters to investigate the performance of a digital communication system. The applicability of these fading models is illustrated by analysing the performance matrices of the digital communication channels in the present work. Various performance matrices such as the average SEP, the channel capacity under different adaptive schemes namely, optimum rate adaptation (ORA), channel inversion with fixed rate (CIFR) and truncated CIFR are derived. The asymptotic analysis of KMIG and EMIG composite fading models over average SEP performance matrices with coding gain and diversity gain is also carried out in this work. The simplified high and low signal-to-noise-ratio solutions to channel capacity are also provided as a by-product. In addition, approximate analysis to ORA and CIFR capacity are provided under realistic environmental conditions. The accuracy of the derived numerical formulations is validated with the use of Monte–Carlo simulation. The results of present work will be advantageous in the modelling and designing of popular wireless services such as vehicle-to-vehicle communication, wearable communication and wireless power transfer related technologies.

**Keywords** Channel capacity · Composite fading distributions · Error probability · Multipath · Shadowing

## 1 Introduction

The need of high data rate and continuous services is increasing day by day with the proliferation of wireless communication systems [1–4]. The quality of a wireless communication system is severely degraded by a physical phenomenon known as fading [5–7]. Multipath and shadowing are two detrimental effects on the quality of radio signals received during wireless propagation [8, 9].

Therefore, there is a requirement of precise modelling of the wireless system for faithful realization of the earlier services and to get improved and reliable performance. In recent years, numerous fading models were proposed by researchers across the globe to meticulously design the wireless systems [10–16]. The signals from various components or routes meet at the receiver with different gains and phases contribute in fading, is known as multipath fading [17–19]. On the other hand, the shadowing results in low speed changes of the mean signal power, which is attributed by the topographical obstacles such as trees, buildings along the path of the transmitter (Tx) and receiver (Rx) [20–30].

The short term (small scale) signal fluctuations also termed as multipath fading are modelled by the well-known models such as Rayleigh, Rice (Nakagami- $n$ ), Hoyt, Nakagami- $m$ , and Weibull distributions. More specifically,

✉ Sanjay Kumar Soni  
sanjoo.ksoni@gmail.com

<sup>1</sup> Tula's Institute, Dehradun, India

<sup>2</sup> M. M. M. University of Technology, Gorakhpur, India

<sup>3</sup> G.B.Pant Institute of Engineering and Technology, Pauri, India

these models are used for modelling of non-line-of-sight (NLOS) scenarios, whereas Rician is used for line-of-sight (LOS) components. In past years, researchers have proposed some new versatile and flexible models namely  $\kappa - \mu$ ,  $\eta - \mu$  and  $\alpha - \mu$  to precisely analyze the effect of small scale fading on the wireless channel. Furthermore, these models can be modified to other convincing multipath distributions like Rayleigh, Rice (Nakagami- $n$ ), one-sided Gaussian distributions by simple remodelling the fading parameters [14, 17–19].

In the last few decades, the log-normal (LN) distribution was the high priority choice of the research community to model the effect of shadowing in the wireless propagation environment [6]. A great magnitude of research has been done so far in the domain of wireless system performance analysis such as bit error rate and channel capacity analysis over LN distribution [20–27]. The LN distribution also finds its usage in satellite communication, radar communication to analyze the effect of fading and also in the field of statistics [24, 25]. Despite of the wide popularity of the LN, it is not much used by the researchers in composite fading statistics due to its difficult mathematical representation which results in numerical intractability [20, 27, 28]. A substitute of LN known as Gamma distribution, used for modelling of shadowing effect in realistic environment such as  $\kappa - \mu$ /Gamma,  $\eta - \mu$ /Gamma have been proposed in [31–36]. In [37] and [38], authors have investigated the performance of communication system where shadowing is modelled with the use of gamma distribution. Although the Gamma distribution has well ordered mathematical structure, it does not match the long-tailed characteristics of LN distribution especially at the high standard deviations [6].

Another distribution which shows near harmony with the LN at high standard deviations is inverse gaussian (IG) distribution [28, 39]. Although IG is highly suitable with the LN distribution, but it fails in finding the exact closed-form module for the analysis of wireless channel such as optimum rate adaptation (ORA) capacity analysis and probability density function (PDF) with selection combining diversity scheme [28]. Most of the composite fading structures proposed by the research community with gamma and IG distributions are expressed in either finite/infinite series representations or sum of mixture of Gamma and IG distributions, respectively [6]. Recently, a new model which ensues the long-tailed characteristics of LN distribution and has a sound competency over the gamma and IG, known as inverse gamma (IGamma) distribution is discussed in [6, 40, 41]. Apart from the communication, the utility of the IGamma is also exploited in other fields such as statistics, mathematics, and science [42]. In [29], authors have justified the utility of inverse gamma in investigating the performance of wireless system where shadowing is

predominant. Authors also used the empirical measurements for performing set of goodness-of-fit tests which supports the claim of inverse gamma distribution for characterizing the shadowing effect in wireless channel modelling. The research has been validated with the help of the Cramer-von Mises test. In [6], authors have performed the comparison of inverse gamma distribution with other shadowed fading distributions based on the moment matching methods together with the Kullback–Leibler divergence for different fading scenarios.

The joint effect of shadowing and multipath must be taken into consideration for the realistic modelling of the digital communication systems. In such practical scenarios, composite fading models are best fitted to analyze the outcomes of the communication system in a more realistic environment where multipath fading and shadowing co-exists [14]. O. S. Badarneh in [43] suggested  $\alpha$ - $\eta$ - $\mathcal{F}$  and  $\alpha$ - $\kappa$ - $\mathcal{F}$  composite fading distributions. In [44], authors have evaluated the capacity of the channel over the  $\mathcal{F}$  composite fading channel. The performance analysis of mobile receiver with random way point mobility in internet of thing network is examined over composite  $\mathcal{F}$  fading model by Badarneh et al. in [45]. In [46], authors have used Fisher-Snedecor  $\mathcal{F}$  composite fading models for analysing the performance of a Non-Orthogonal Multiple Access (NOMA) network. Bithas et al. in [47] have suggested a new composite fading model to describe the received signal characteristics in Unmanned Aerial Vehicle (UAV)-enabled communications scenario where shadowing co-exists with the single and double-scattering propagation.

Open literature is flooded with many composite fading models and every model has its merits and demerits. A single fading model cannot be justifiable for each fading scenario. The composite fading distributions available in the literature lag in rendering extensive modelling of the fading phenomenon. Moreover, there have been various composite fading models based on different shadowing and multipath fading distributions. However, these models lead to the ambiguity in various performance matrices of interest. In last few years some composite models using IGamma for characterizing shadowing such as the KMIG and EMIG have been proposed by the researchers [14, 15].

The fundamental statistics of KMIG and EMIG composite fading models are explored in [40, 41], where the authors have supported their work by the vast experimental measurements in terms of traditional and growing wireless applications. These applications includes vehicular and wearable communication systems. The tractable solutions of various analyses are also possible due to their straight mathematical structure. In [41, 48, 49], the analytical expressions for ergodic capacity and coherent bit error rate for multiple amplitude modulation format are discussed over aforementioned composite fading channels. The

results are obtained in infinite summation terms, thus truncation error is also included.

To the best of our knowledge, the available literature has a huge scope in extensive performance investigation of the digital communication system with inverse gamma shadowing based composite fading models. Keeping in view of the above facts, the following performance investigation of the digital communication system are carried out in this work:

- Unified analytical expressions for the average SEP with coherent and non-coherent modulation schemes.
- The earlier proposed formulations contain infinite series representation, thus truncation error is also provided.
- Asymptotic analysis is also provided for previously discussed performance matrices along with coding and diversity gains.
- Analytical expressions for the ORA, CIFR, and TIFR channel capacity are derived.
- The expressions for ORA capacity contain single infinite summation term, whereas the expressions proposed in [41, 48] have multiple summation terms and valid for integer parameters of  $m_s$ .
- The closed-form results obtained under CIFR policy do not show any impact of shadowing as the mathematical notations are independent of shadowing parameter  $m_s$ .
- Channel capacity analysis is also done with low and high power to visualise and subsequently gain more physical insight to the system performance.
- Further, ORA and CIFR results are simplified under different fading conditions.

The remaining part of work is organized as follows. The structure of KMIG and EMIG composite fading models are explained in the Sect. 2. Performance evaluation under average symbol error probability of composite fading distributions are given in Sect. 3. Asymptotic analysis is carried out in Sect. 4. Channel capacity analysis under various adaptive schemes like ORA, CIFR, and TIFR is given in Sect. 5. Section 6 deals with the result and discussion. Finally, the concluding remark has been made in Sect. 7.

## 2 Statistics of KPIG and EMIG composite fading models

For  $\kappa, \mu, m_s, \gamma, \bar{\gamma} \in R^+$ , the instantaneous signal-to-noise-ratio (SNR) PDF of KPIG composite distribution is given as [40]

$$f_Y(\gamma) = \frac{\exp(-\mu\kappa)\mu^\mu(\kappa + 1)^\mu(m_s\bar{\gamma})^{m_s}\gamma^{\mu-1}}{B(m_s, \mu)[\mu(\kappa + 1)\gamma + m_s\bar{\gamma}]^{m_s+\mu}} \times {}_1F_1\left[m_s + \mu; \mu; \frac{\mu^2\kappa(\kappa + 1)\gamma}{\mu(\kappa + 1)\gamma + m_s\bar{\gamma}}\right] \tag{1}$$

where  $B(\cdot)$  signifies the Beta function [50, Eq. (8.384.1)] and  ${}_1F_1(\cdot; \cdot; \cdot)$  denotes the confluent hypergeometric function [50, Eq. (9.210.1)]. Invoking the identity [51, Eq. (07.20.02.0001.01)], (1) can be re-written as

$$f_Y(\gamma) = \sum_{r=0}^{\infty} \frac{(m_s + \mu)_r (\mu\kappa)^r \exp(-\mu\kappa) \mu^{\mu+r} (\kappa + 1)^{\mu+r} (m_s\bar{\gamma})^{m_s} \gamma^{\mu+r-1}}{r! (\mu)_r B(m_s, \mu) [\mu(\kappa + 1)\gamma + m_s\bar{\gamma}]^{m_s+\mu+r}} \tag{2}$$

where  $(\cdot)_r$  represents the Pochhammer symbol [51, Eq. (06.10.02.0001.01)].

For  $\eta, \mu, m_s, \gamma, \bar{\gamma} \in R^+$ , the instantaneous SNR PDF of EMIG composite distribution is expressed as [40, Eq. (13)]

$$f_Y(\gamma) = \frac{2^{2\mu} \mu^{2\mu} h^\mu (m_s\bar{\gamma})^{m_s} \gamma^{2\mu-1}}{B(m_s, 2\mu) (2\mu h\gamma + m_s\bar{\gamma})^{m_s+2\mu}} \times {}_2F_1\left(\frac{m_s + 2\mu}{2}, \frac{m_s + 2\mu + 1}{2}; \frac{2\mu + 1}{2}; \frac{(2\mu H\gamma)^2}{(2\mu h\gamma + m_s\bar{\gamma})^2}\right) \tag{3}$$

By utilising [51, Eq. (07.20.02.0001.01)], the PDF given by (3) can be re-written as

$$f_Y(\gamma) = \sum_{r=0}^{\infty} \frac{\left(\frac{m_s+2\mu}{2}\right)_r \left(\frac{m_s+2\mu+1}{2}\right)_r (2\mu H\gamma)^{2r} 2^{2\mu} \mu^{2\mu} h^\mu (m_s\bar{\gamma})^{m_s} \gamma^{2\mu-1}}{r! \left(\frac{2\mu+1}{2}\right)_r (2\mu h\gamma + m_s\bar{\gamma})^{2r} B(m_s, 2\mu) (2\mu h\gamma + m_s\bar{\gamma})^{m_s+2\mu}} \tag{4}$$

For both distributions, shadowing is associated with the scale parameter given by  $m_s$ . On the other hand,  $\kappa$  (total dominant to scattered power ratio),  $\mu$  (number of multipath clusters arriving at the receivers), and  $\eta$  have two alternate formats, where in *format – I*,  $\eta$  is given as the ratio of scattered wave power between the in-phase and quadrature components of each bunch of multipath with  $h = (2 + \eta^{-1} + \eta)/4$  and  $H = (\eta^{-1} - \eta)/4$ . On the contrary,  $\eta$  is defined as the correlation coefficient between the in-phase and quadrature components in *format – II* [40] with  $h = 1/(1 - \eta^2)$  and  $H = \eta/(1 - \eta^2)$  are the multipath parameters. In the present paper, *format – I* is used while using the EMIG composite fading distribution for investigating the various performance matrices.

### 3 Average symbol error probability

The straightforward methodology to derive the average SEP of a fading channel, is to take ensemble average of the conditional SEP over fading SNR,  $\gamma$  [28]

$$\bar{P}_e = \int_0^\infty P_e(\gamma) f_Y(\gamma) d\gamma \tag{5}$$

where  $P_e(\gamma)$  is  $\gamma$ -dependent instantaneous symbol error rate (SER) of the modulation techniques [6, Eq. (17)].

#### 3.1 ASEP of coherent modulation scheme

The generalised expression of the probability of error for the coherent modulation schemes over additive white Gaussian noise (AWGN) channel is given by [6, Eq. (18)]

$$P_e(\gamma) = A_p \operatorname{erfc}(\sqrt{B_p \gamma}) \tag{6}$$

where  $\operatorname{erfc}(\cdot)$  is the complementary error function and the values of  $A_p$  and  $B_p$  for different modulation schemes are given in [52, Table I].

##### 3.1.1 ASEP of coherent modulation scheme for KMIG composite fading model

By putting the value of (2) and (6) into (5), one obtains

$$\begin{aligned} \bar{P}_e^{coh} &= \sum_{r=0}^\infty \frac{(m_s + \mu)_r (\mu\kappa)^r \exp(-\mu\kappa) \mu^{\mu+r} (\kappa + 1)^{\mu+r} (m_s \bar{\gamma})^{m_s}}{r! (\mu)_r B(m_s, \mu)} \\ &\times A_p \int_0^\infty \frac{\gamma^{\mu+r-1} \operatorname{erfc}(\sqrt{B_p \gamma})}{[\mu(\kappa + 1)\gamma + m_s \bar{\gamma}]^{m_s + \mu + r}} d\gamma \end{aligned} \tag{7}$$

Employing simple variable transformation along with the identity [53, Eq. (2.8.3.4)], (7) can be written as

$$\begin{aligned} \bar{P}_e^{coh} &= \sum_{r=0}^\infty \frac{(m_s + \mu)_r (\mu\kappa)^r \exp(-\mu\kappa) (\mu(\kappa + 1))^{\mu+r} A_p}{r! (\mu)_r B(m_s, \mu) \sqrt{\pi} (\mu + r) (B_p m_s \bar{\gamma})^{\mu+r}} \\ &\times \Gamma\left(\frac{2\mu + 2r + 1}{2}\right) \\ &{}_3F_1\left(m_s + \mu + r, \mu + r, \mu + r + \frac{1}{2}; \mu + r + 1; \frac{-\mu(\kappa + 1)}{B_p m_s \bar{\gamma}}\right) \end{aligned} \tag{8}$$

where  ${}_pF_q(\cdot, \cdot)$  is the generalised hypergeometric function [50]. The above expression is analytical solution of the

average SEP of KMIG composite fading model for different coherent modulation schemes, where  $\Gamma(\cdot)$  denotes the Gamma function [50, Eq. (8.310.1)]. Truncating the infinite series given by (8) after  $p - 1$  terms, one obtains the following error metric

$$\begin{aligned} T &= \sum_{r=p}^\infty \frac{(m_s + \mu)_r (\mu\kappa)^r \exp(-\mu\kappa) (\mu(\kappa + 1))^{\mu+r} A_p}{r! (\mu)_r B(m_s, \mu) \sqrt{\pi} (\mu + r) (B_p m_s \bar{\gamma})^{\mu+r}} \\ &\times \Gamma\left(\frac{2\mu + 2r + 1}{2}\right) \\ &{}_3F_1\left(m_s + \mu + r, \mu + r, \mu + r + \frac{1}{2}; \mu + r + 1; \frac{-\mu(\kappa + 1)}{B_p m_s \bar{\gamma}}\right) \end{aligned} \tag{9}$$

Both Gauss hypergeometric and Gamma functions in (9) have monotonically decreasing nature with respect to  $r$ , then (9) can be upper bounded by the inequality as given below with the use of basic definitions of pochhammer symbol and gamma function [54, 55]

$$\begin{aligned} T &\leq \frac{A_p \exp(-\mu\kappa) (\mu(\kappa + 1))^\mu \Gamma(\mu + \frac{1}{2})}{\mu \sqrt{\pi} B(m_s, \mu) (B_p m_s \bar{\gamma})^\mu} \\ &\sum_{r=0}^\infty \frac{(m_s + \mu)_r (\mu + \frac{1}{2})_r}{r! (\mu + 1)_r} \\ &\left(\frac{\mu^2 \kappa (\kappa + 1)}{B_p m_s \bar{\gamma}}\right)^r \\ &\times {}_3F_1\left(m_s + \mu + p, \mu + p, \mu + p + \frac{1}{2}; \mu + p + 1; \frac{-\mu(\kappa + 1)}{B_p m_s \bar{\gamma}}\right) \end{aligned} \tag{10}$$

The infinite series expression in the above equation(10) can be represented in closed-form upper bound with the use of generalized hypergeometric function [50] as follows

$$\begin{aligned} T &\leq \frac{A_p \exp(-\mu\kappa) (\mu(\kappa + 1))^\mu \Gamma(\mu + \frac{1}{2})}{\mu \sqrt{\pi} B(m_s, \mu) (B_p m_s \bar{\gamma})^\mu} \\ &{}_2F_1\left(m_s + \mu, \mu + \frac{1}{2}; \mu + 1, \frac{\mu^2 (\kappa + 1)}{B_p m_s \bar{\gamma}}\right) \\ &\times {}_3F_1\left(m_s + \mu + p, \mu + p, \mu + p + \frac{1}{2}; \mu + p + 1; \frac{-\mu(\kappa + 1)}{B_p m_s \bar{\gamma}}\right) \end{aligned} \tag{11}$$

##### 3.1.2 ASEP of coherent modulation scheme for EMIG composite fading model

By putting the value of (4) and (6) into (5) and after certain simple mathematical manipulations, one obtains

$$\bar{P}_e^{coh} = \sum_{r=0}^{\infty} \frac{A_p(2\mu)^{2\mu+2r} h^\mu H^{2r}(m_s \bar{\gamma})^{m_s} \left(\frac{m_s+2\mu}{2}\right)_r \left(\frac{m_s+2\mu+1}{2}\right)_r}{r! B(m_s, 2\mu) \left(\frac{2\mu+1}{2}\right)_r} \times \int_0^{\infty} \frac{\gamma^{2\mu+2r-1} \operatorname{erfc}(\sqrt{B_p \gamma})}{(2\mu h \gamma + m_s \bar{\gamma})^{m_s+2\mu+2r}} d\gamma \tag{12}$$

After necessary change of variables in integral part of (12) and following the similar approach as in Sect. 3.1.1, it insinuates

$$\bar{P}_e^{coh} = \sum_{r=0}^{\infty} \frac{A_p(2\mu)^{2\mu+2r} h^\mu H^{2r} \Gamma(\mu+r) \Gamma\left(\frac{4\mu+4r+1}{2}\right)}{2\sqrt{\pi} r! \Gamma(\mu) B(m_s, 2\mu+2r) (\mu+r) (B_p m_s \bar{\gamma})^{2\mu+2r}} \times {}_3F_1\left(m_s+2\mu+2r, 2\mu+2r, \frac{4\mu+4r+1}{2}; 2\mu+2r+1; \frac{-2\mu h}{B_p m_s \bar{\gamma}}\right) \tag{13}$$

Truncating the infinite series given by (13) with  $p$  number of terms, results to the following error metric

$$T = \frac{A_p(2\mu)^{2\mu} h^\mu}{2\sqrt{\pi} \Gamma(\mu) (B_p m_s \bar{\gamma})^{2\mu}} \sum_{r=p}^{\infty} \frac{\Gamma(\mu+r) \Gamma\left(\frac{4\mu+4r+1}{2}\right)}{r! B(m_s, 2\mu+2r) (\mu+r) \left(\frac{2\mu H}{B_p m_s \bar{\gamma}}\right)^{2r}} \times {}_3F_1\left(m_s+2\mu+2r, 2\mu+2r, \frac{4\mu+4r+1}{2}; 2\mu+2r+1; \frac{-2\mu h}{B_p m_s \bar{\gamma}}\right) \tag{14}$$

After following the similar approach as in the 3.1.1, the closed-form upper bound expression for the truncation error in (14) is given as follows

$$T \leq \frac{A_p(2\mu)^{2\mu-1} h^\mu}{\sqrt{\pi} (B_p m_s \bar{\gamma})^{2\mu} B(m_s, 2\mu)} \times {}_3F_1\left(m_s+2\mu+2p, 2\mu+2p, 2\mu+2p+\frac{1}{2}; 2\mu+2p+1; \frac{-2\mu h}{B_p m_s \bar{\gamma}}\right) \times {}_4F_2\left(\mu+\frac{1}{4}, \mu+\frac{3}{4}, \frac{m_s+2\mu+1}{2}, \mu; \mu+\frac{1}{2}, \mu+1; \left(\frac{4\mu h}{B_p m_s \bar{\gamma}}\right)^2\right) \tag{15}$$

### 3.2 ASEP of non-coherent modulation scheme

Sometimes, it becomes tedious to trace the phase of the received signal while analysing the performance of a communication system. In such cases, non-coherent modulation schemes play a pivotal role in the faithful implementation of the system. In the past, a lot of research has been done in the field of non-coherent modulation schemes for different fading channels [27, 28, 56, 57]. In the following sections, we presents the analytical solutions for different non-coherent schemes over aforementioned composite fading models. The instantaneous SEP expression for non-coherent policies is defined as [6, Eq. (26)]

$$P_e(\gamma) = A_n \exp(-B_n \gamma) \tag{16}$$

where the parameters  $A_n$  and  $B_n$  covering a wide range of non-coherent modulation formats are listed in [56, Table 2].

#### 3.2.1 ASEP of non-coherent modulation scheme of KMIG

By using the PDF of KMIG given in (2) and (16) into (5), it results

$$\bar{P}_e^{NCoh} = \sum_{r=0}^{\infty} \frac{(m_s + \mu)_r (\mu \kappa)^r \exp(-\mu \kappa) \mu^{\mu+r} (\kappa + 1)^{\mu+r} (m_s \bar{\gamma})^{m_s} A_n}{r! (\mu)_r B(m_s, \mu)} \times \int_0^{\infty} \frac{\gamma^{\mu+r-1} \exp(-B_n \gamma)}{[\mu(\kappa+1)\gamma + m_s \bar{\gamma}]^{m_s+\mu+r}} d\gamma \tag{17}$$

Now, employing the identity [55, Eq. (2.3.6.9)] and [50, Eq. (9.210.2)], (17) can be written in simplified form as

$$\bar{P}_e^{NCoh} = \sum_{r=0}^{\infty} \frac{(\mu \kappa)^r}{r! \exp(\mu \kappa)} \left\{ \begin{aligned} & {}_1F_1\left(\mu+r; 1-m_s; \frac{B_n m_s \bar{\gamma}}{\mu(\kappa+1)}\right) \\ & + \left\{ \begin{aligned} & \left[\frac{B_n m_s \bar{\gamma}}{\mu(\kappa+1)}\right]^{m_s} \frac{\Gamma(-m_s)}{B(m_s, \mu+r)} \\ & {}_1F_1\left(m_s+\mu+r; m_s+1; \frac{B_n m_s \bar{\gamma}}{\mu(\kappa+1)}\right) \end{aligned} \right. \end{aligned} \right. \tag{18}$$

Truncating the infinite series given by (18) with  $p$  number of terms, will results in the following truncation error metric

$$T = \sum_{r=p}^{\infty} \frac{(\mu\kappa)^r}{r! \exp(\mu\kappa)} \left\{ \begin{aligned} & {}_1F_1\left(\mu + r; 1 - m_s; \frac{B_n m_s \bar{\gamma}}{\mu(\kappa + 1)}\right) \\ & + \left\{ \left[ \frac{B_n m_s \bar{\gamma}}{\mu(\kappa + 1)} \right]^{m_s} \frac{\Gamma(-m_s)}{B(m_s, \mu + r)} \right. \\ & \left. + {}_1F_1\left(m_s + \mu + r; m_s + 1; \frac{B_n m_s \bar{\gamma}}{\mu(\kappa + 1)}\right) \right\} \end{aligned} \right. \quad (19)$$

Following the similar approach as in the Sect. 3.1.1 and with the use of generalized hypergeometric functions [50], the closed-form upper bound expression for the truncation error of (18) can be given by following inequality

$$T \leq \exp(-\mu\kappa) {}_1F_1\left(\mu + p; 1 - m_s; \frac{B_n m_s \bar{\gamma}}{\mu(\kappa + 1)}\right) {}_1F_1(1; 1; \mu\kappa) + \frac{e^{-\mu\kappa} \Gamma(-m_s)}{B(m_s, \mu)} \times \left(\frac{B_n m_s \bar{\gamma}}{\mu(\kappa + 1)}\right)^{m_s} {}_1F_1\left(m_s + \mu + p; m_s + 1; \frac{B_n m_s \bar{\gamma}}{\mu(\kappa + 1)}\right) {}_1F_1(m_s + \mu; \mu; \mu\kappa) \quad (20)$$

### 3.2.2 ASEP of non-coherent modulation scheme of EMIG

Substituting the PDF of EMIG given by (4) and (16) into (5), with following the same approach as in Sect. 3.2.1, it follows

$$\bar{P}_e^{NCoh} = \sum_{r=0}^{\infty} \frac{A_n \Gamma(\mu + r) H^{2r}}{r! \Gamma(\mu) h^{\mu+2r}} \left\{ \begin{aligned} & {}_1F_1\left(2\mu + 2r; 1 - m_s; \frac{B_n m_s \bar{\gamma}}{2\mu h}\right) \\ & + \left\{ \left(\frac{B_n m_s \bar{\gamma}}{2\mu h}\right)^{m_s} \frac{\Gamma(-m_s)}{B(m_s, 2\mu + 2r)} \right. \\ & \left. + {}_1F_1\left(m_s + 2\mu + 2r; 1 - m_s; \frac{B_n m_s \bar{\gamma}}{2\mu h}\right) \right\} \end{aligned} \right. \quad (21)$$

The truncation error for infinite series representation given by (21) is obtained while truncating it to  $p$  number of terms, it follows

$$T = \sum_{r=p}^{\infty} \frac{A_n \Gamma(\mu + r) H^{2r}}{r! \Gamma(\mu) h^{\mu+2r}} \left\{ \begin{aligned} & {}_1F_1\left(2\mu + 2r; 1 - m_s; \frac{B_n m_s \bar{\gamma}}{2\mu h}\right) \\ & + \left\{ \left(\frac{B_n m_s \bar{\gamma}}{2\mu h}\right)^{m_s} \frac{\Gamma(-m_s)}{B(m_s, 2\mu + 2r)} \right. \\ & \left. + {}_1F_1\left(m_s + 2\mu + 2r; 1 - m_s; \frac{B_n m_s \bar{\gamma}}{2\mu h}\right) \right\} \end{aligned} \right. \quad (22)$$

With the same methodology as in the Sect. 3.1.1 and with the use of generalized hypergeometric functions [50], the closed-form upper bound expression for the truncation error of (21) can be given by following inequality

$$T \leq \frac{A_n}{h^\mu} {}_1F_1\left(2\mu + 2p; 1 - m_s; \frac{B_n m_s \bar{\gamma}}{2\mu h}\right) {}_2F_1\left(\mu, 1; 1; \frac{H^2}{h^2}\right) + \frac{A_n \Gamma(-m_s) \Gamma(m_s + 2\mu)}{h^\mu \Gamma(2\mu)} \left(\frac{B_n m_s \bar{\gamma}}{2\mu h}\right)^{m_s} {}_1F_1\left(m_s + 2\mu + 2p; 1 - m_s; \frac{B_n m_s \bar{\gamma}}{2\mu h}\right) \times {}_2F_1\left(\frac{m_s + 2\mu}{2}, \frac{m_s + 2\mu + 1}{2}; \frac{2\mu + 1}{2}; \frac{H^2}{h^2}\right) \quad (23)$$

## 4 Asymptotic analysis

Asymptotic analysis is one of the vital analysis of the wireless communication system at high SNR. This helps in predicting the slope and shifting of the curve. It also assist in investigating the different performance metrics of the digital communication channel in the absence and presence of the diversity [58, 59] in a convenient way. In the following sections, we present the origin envelope as well as power PDFs of KMIG and EMIG composite fading models. Closed-form asymptotic solutions of BER for the aforementioned composite fading models is also presented.

### 4.1 Origin PDF of KMIG

The origin envelope PDF of  $\kappa - \mu$  distribution is well defined in [59] as

$$f_X(x) \approx \frac{2\mu^\mu (\kappa + 1)^\mu x^{2\mu-1}}{\Gamma(\mu) \exp(\mu\kappa) \bar{x}^{2\mu}} + \varphi \quad (24)$$

where  $\varphi$  is the higher order terms. The IGamma random variable (RV) with shape parameter  $m_s$  and scale parameter  $\frac{m_s}{\Omega_s}$ , where  $\Omega_s$  is set equal to unity (i.e.  $\Omega_s = 1$ ) [14] is given as follows

$$f_W(w) = \frac{m_s^{m_s}}{\Gamma(m_s)} w^{-m_s-1} \exp\left(\frac{-m_s}{w}\right) \tag{25}$$

The composite envelope PDF of KMIG channel at origin is calculated by averaging conditional PDF of  $\kappa - \mu$  fading distribution with respect to random variations of mean signal power of IGamma fading distribution [14] as follows

$$f_X(x) \approx \int_0^\infty \frac{2\mu^\mu(1+\kappa)^\mu x^{2\mu-1} m_s^{m_s} w^{-m_s-1}}{\Gamma(\mu)\Gamma(m_s)e^{\mu\kappa}(\sqrt{w})^{2\mu}} \exp\left(\frac{-m_s}{w}\right) dw + \varphi \tag{26}$$

Applying transformation of variables and with the inclusion of the identity [50, Eq. 2.3.3.1], the above expression is modified as

$$f_X(x) \approx \frac{2\mu^\mu(1+\kappa)^\mu x^{2\mu-1}}{m_s^\mu e^{\mu\kappa} B(m_s, \mu)} + \varphi \tag{27}$$

The expression for origin SNR density function of the KMIG distribution is obtained by the use of [60, Eq. (2.3)]

$$f_Y(\gamma)^{asym} \approx P\gamma^{Q-1} + \varphi \tag{28}$$

where  $P = \frac{\mu^\mu(1+\kappa)^\mu}{m_s^\mu e^{\mu\kappa} B(m_s, \mu)}$  and  $Q = \mu$ .

### 4.2 Origin PDF of EMIG

The origin envelope PDF of  $\eta - \mu$  distribution is given in [59] as

$$f_X(x) \approx \frac{4\sqrt{\pi}\mu^{2\mu}h^\mu x^{4\mu-1}}{\Gamma(\mu)\Gamma(\mu+\frac{1}{2})x^{4\mu}} + \varphi \tag{29}$$

with the use of similar method as in previous Sect. 4.1, the power PDF of EMIG in closed-form can be written as

$$f_Y(\gamma)^{asym} \approx A\gamma^{B-1} + \varphi \tag{30}$$

where  $A = \frac{2\sqrt{\pi}\mu^{2\mu}h^\mu\Gamma(m_s+2\mu)}{\Gamma(\mu)\Gamma(m_s)\Gamma(\mu+\frac{1}{2})m_s^{2\mu}}$  and  $B = 2\mu$ .

### 4.3 Coherent ASEP

Substituting (28) and (6) into (5) and by utilising the identity [53, Eq. 2.8.2.1], one can find the closed-form asymptotic solution of the KMIG composite fading channel for coherent average SEP

$$\bar{P}_e^{coh,asym} \approx \frac{A_p P \Gamma(\frac{2\mu+1}{2})}{\sqrt{\pi} Q (B_p \gamma_s)^Q} \tag{31}$$

In the above expression (31),  $\gamma_s = \frac{E_s}{N_0}$  is the unfaded SNR, where  $E_s$  is the energy per symbol,  $N_0$  is the one-sided

power spectral density of AWGN channel. Similarly, the closed-form asymptotic solution of EMIG fading channel is obtained by plugging (30) and (6) into (5) and by utilising the identity [53, Eq. 2.8.2.1] as

$$\bar{P}_e^{coh,asym} \approx \frac{A_p A \Gamma(\frac{4\mu+1}{2})}{\sqrt{\pi} B (B_p \gamma_s)^B} \tag{32}$$

In [61], Wang and Giannakis illustrated that diversity gain (DG) and coding gain (CG) can be employed for the characterization of average SEP. Authors has also suggested that these gains are influenced by the asymptotic power PDF around the origin. Furthermore, CG and DG can be calculated in the following manner

$$P_e = (G_c \bar{\gamma})^{-G_d} \tag{33}$$

where  $G_c$  is the CG and  $G_d$  is the DG [61]. So comparing (32) with (33), for the coherent modulation scheme over KMIG, the DG is given as  $G_d = \mu$ , where the CG is given as follows

$$G_c = B_p \left( \frac{\sqrt{\pi}\mu}{A_p P \Gamma(\frac{2\mu+1}{2})} \right)^{\frac{1}{\mu}} \tag{34}$$

Similarly for EMIG, the DG is given as  $G_d = 2\mu$ , where the CG is given as follows

$$G_c = B_p \left( \frac{\sqrt{\pi}2\mu}{A_p A \Gamma(\frac{4\mu+1}{2})} \right)^{\frac{1}{2\mu}} \tag{35}$$

### 4.4 Non-coherent ASEP

By putting (28) and (16) into (5) and with the use of [50, Eq. 3.381.4], one can obtain the closed-form solution over KMIG as follows

$$\bar{P}_e^{Ncoh,asym} \approx \frac{A_n P \Gamma(Q)}{(B_n \gamma_s)^Q} \tag{36}$$

Similarly, the closed-form expression of EMIG composite fading channel for non-coherent average SEP can be obtained by putting (30) and (16) into (5) and by the use of identity [50, Eq. 3.381.4] as follows

$$\bar{P}_e^{Ncoh,asym} \approx \frac{A_n A \Gamma(B)}{(B_n \gamma_s)^B} \tag{37}$$

So with the use of (36) in (33), the DG over KMIG is given by  $G_d = \mu$ , where the CG is given as follows

$$G_c = \frac{B_n}{(A_p P \Gamma(\mu))^{\frac{1}{\mu}}} \tag{38}$$

Similarly for the EMIG the DG and CG are given by comparing (37) with (33), which gives  $G_d = 2\mu$  and CG is given as follows

$$G_c = \frac{B_n}{(A_p A \Gamma(2\mu))^{\frac{1}{2\mu}}} \tag{39}$$

### 5 Channel capacity

Shannon’s channel capacity describe the relation of capacity of a channel in the form of amount of data that a channel can supports with minimum probability of error [28, 30]. The amount of information that a channel can transmit/receive is a function of the fading state of the channel [12, 18]. Capacity of a fading channel reduces if the transmitter power does not changes. Adaptive transmission policies can help in minimizing the effect of fading on channel’s ability to carry the information. Channel state information(CSI) plays a vital role in improving the system efficiency as far as channel capacity is concerned [6, 28]. Different adaptive transmission policies which depends on CSI are given in the following Subsections with complete analysis.

#### 5.1 Optimum rate adaptation

ORA transmission scheme is implemented in the scenario where receiver has the perfect information of the CSI. Transmitter power does not changes and the rate of transmission depends on the channel conditions in the case of ORA scheme. Thus, the ORA transmission policy over a fading SNR is obtained by the following relation [6, 26]

$$C_{ORA} = \int_0^\infty W C_{avgn} f_Y(\gamma) d\gamma \tag{40}$$

where  $C_{avgn} = \log_2(1 + \gamma)$  and channel bandwidth in Hz is represented by  $W$

##### 5.1.1 ORA for KMIG fading model

With the use of (2) in (40) and applying some mathematical manipulations, we find that

$$C_{ORA} = \sum_{r=0}^\infty \frac{W(m_s + \mu)_r (\mu\kappa)^r \exp(-\mu\kappa) (m_s \bar{\gamma})^{m_s}}{r! (\mu)_r B(m_s, \mu) \log(2) [\mu(\kappa + 1)]^{m_s}} \int_0^\infty \frac{\gamma^{\mu+r-1} \log(\gamma + 1)}{\left[\gamma + \frac{\bar{\gamma} m_s}{\mu(1 + \kappa)}\right]^{r+m_s+\mu}} d\gamma \tag{41}$$

By the help of the identity [55, Eq. (2.5.10.56)] in (41), the expression results into

$$C_{ORA} = \sum_{r=0}^\infty \mathcal{A} \left\{ \begin{aligned} &\psi(m_s + \mu + r) - \psi(m_s) \\ &- \left\{ \begin{aligned} &\frac{(\mu + r)}{(m_s + \mu + r)} \left(1 - \frac{m_s \bar{\gamma}}{\mu(\kappa + 1)}\right) \\ &{}_3F_2\left(\mu + r + 1, 1, 1; 2, m_s + \mu + r + 1; 1 - \frac{m_s \bar{\gamma}}{\mu(\kappa + 1)}\right) \end{aligned} \right\} \end{aligned} \right. \tag{42}$$

where

$$\mathcal{A} = \frac{W(m_s + \mu)_r \exp(-\mu\kappa) (\mu\kappa)^r B(\mu + r, m_s)}{r! (\mu)_r B(m_s, \mu) \log(2)}$$

and  $\psi(\cdot)$  is the psi function [50].

The above expression can be further reduced with the help of basic mathematical simplifications [50], the final solution for the ORA can be re-written as

$$C_{ORA} = \sum_{r=0}^\infty \frac{W \exp(\mu\kappa) (\mu\kappa)^r}{r! \log(2)} \left\{ \begin{aligned} &\psi(m_s + \mu + r) - \psi(m_s) \\ &- \left\{ \begin{aligned} &\frac{(\mu + r)}{(m_s + \mu + r)} \left(1 - \frac{m_s \bar{\gamma}}{\mu(\kappa + 1)}\right) \\ &{}_3F_2\left(\mu + r + 1, 1, 1; 2, m_s + \mu + r + 1; 1 - \frac{m_s \bar{\gamma}}{\mu(\kappa + 1)}\right) \end{aligned} \right\} \end{aligned} \right. \tag{43}$$

The above mathematical notation can be further re-expressed under high SNR, deducing (41) at high values of SNR i.e.  $\gamma \gg 1$  such that  $\log_2(1 + \gamma) \approx \log_2(\gamma)$ , one obtains

$$C_{ORA}^{HP} \approx \sum_{r=0}^\infty \frac{W(m_s + \mu)_r (\mu\kappa)^r \exp(-\mu\kappa) (m_s \bar{\gamma})^{m_s}}{r! (\mu)_r B(m_s, \mu) \log(2) [\mu(\kappa + 1)]^{m_s}} \times \int_0^\infty \frac{\gamma^{\mu+r-1} \log(\gamma)}{\left[\gamma + \frac{m_s \bar{\gamma}}{\mu(\kappa + 1)}\right]^{m_s+\mu+r}} d\gamma \tag{44}$$

With the help of the identity [55, Eq. 2.6.4.7], (44) can be re-written as given below

$$C_{ORA}^{HP} \approx \sum_{r=0}^\infty \frac{W \exp(-\mu\kappa) (\mu\kappa)^r}{r! \log(2)} \left( \log\left(\frac{m_s \bar{\gamma}}{\mu(\kappa + 1)}\right) + \psi(\mu + r) - \psi(m_s) \right) \tag{45}$$



Similarly, at the low values of SNR, i.e.  $\gamma < 1$ ,  $\log_2(1 + \gamma) \approx \gamma \log_2(e)$ , now with the use of previous relation in (41), the ORA capacity can be calculated by finding the 1<sup>st</sup> order moment of KMIG distribution by the use of  $n = 1$  in [40, Eq. (8)]

$$C_{ORA}^{LP} \approx \frac{W \log_2(e) m_s \bar{\gamma} \exp(-\mu\kappa) B(m_s - 1, \mu + 1)}{\mu(\kappa + 1) B(m_s, \mu)} {}_1F_1(\mu + 1, \mu, \mu\kappa) \tag{46}$$

With some basic mathematical manipulation, the above solution can be modified as given below

$$C_{ORA}^{LP} \approx \frac{W \log_2(e) m_s \bar{\gamma} \exp(-\mu\kappa)}{(\kappa + 1)(m_s - 1)} {}_1F_1(\mu + 1, \mu, \mu\kappa) \tag{47}$$

Further, at  $m_s \gg 1$  (47) reduced to

$$C_{ORA}^{LP} \approx \frac{W \log_2(e) \bar{\gamma} \exp(-\mu\kappa)}{(\kappa + 1)} {}_1F_1(\mu + 1, \mu, \mu\kappa) \tag{48}$$

### 5.1.2 ORA for EMIG fading model

Substituting the PDF relation (4) into (40) and following similar step as in Sect. 5.1.1, one obtains

$$C_{ORA} = \sum_{r=0}^{\infty} \frac{W \binom{m_s+2\mu}{2} \binom{m_s+2\mu+1}{2} H^{2r} (m_s \bar{\gamma})^{m_s}}{r! \binom{2\mu+1}{2} B(m_s, 2\mu) \log(2) (2\mu)^{m_s} h^{m_s+\mu+2r}} \times \int_0^{\infty} \frac{\gamma^{2\mu+2r-1} \log(\gamma + 1)}{(\gamma + \frac{m_s \bar{\gamma}}{2\mu h})^{2\mu+2r+m_s}} d\gamma \tag{49}$$

By the help of the identity [55], the above expression can be re-written as

$$C_{ORA} = \sum_{r=0}^{\infty} \hat{A} \begin{cases} \psi(m_s + 2\mu + 2r) - \psi(m_s) \\ \frac{(2\mu + 2r)}{(m_s + 2\mu + 2r)} \left(1 - \frac{m_s \bar{\gamma}}{2\mu h}\right) \\ {}_3F_2\left(2\mu + 2r + 1, 1, 1; 2, 2\mu + 2r + m_s + 1; 1 - \frac{m_s \bar{\gamma}}{2\mu h}\right) \end{cases} \tag{50}$$

where  $\hat{A} = \frac{W\Gamma(\mu + r)H^{2r}}{r!\Gamma(\mu)\log(2)h^{\mu+2r}}$ .

By following the same method as in the Sect. 5.1.1, the above expression at high values of SNR can be re-written as

$$C_{ORA}^{HP} \approx \sum_{r=0}^{\infty} \frac{W\Gamma(\mu + r)H^{2r}}{r!\Gamma(\mu)\log(2)h^{\mu+2r}} \left[ \log\left(\frac{m_s \bar{\gamma}}{2\mu h}\right) + \psi(2\mu + 2r) - \psi(m_s) \right] \tag{51}$$

The solution to ORA capacity at low SNR is determined by evaluating the 1<sup>st</sup> order moment of the EMIG distribution [40, Eq. (19)]

$$C_{ORA}^{LP} \approx \frac{W \log_2(e) m_s \bar{\gamma}}{(m_s - 1) h^{\mu+1}} {}_2F_1\left(\mu + \frac{1}{2}, \mu + 1; \mu + \frac{1}{2}; \frac{H^2}{h^2}\right) \tag{52}$$

Similar to KMIG, (52) at high value of shadowing parameters  $m_s$  takes the structure

$$C_{ORA}^{LP} \approx \frac{W \log_2(e) \bar{\gamma}}{h^{\mu+1}} {}_2F_1\left(\mu + \frac{1}{2}, \mu + 1; \mu + \frac{1}{2}; \frac{H^2}{h^2}\right) \tag{53}$$

The approximate expressions given by (48) and (53) are evolved while considering  $m_s \gg 1$ , as quite prominent case seen in the practical urban scenarios. These results are independent of shadowing parameter and thus set the lower limit of the spectral efficiency (i.e. minimum achievable capacity) in terms of  $m_s$  under low-power regime and similar observation can be made from the Fig. 1. The above derived expressions have generic nature, thus can be transformed to the ergodic capacity analysis for variety of fading distributions by selecting suitable values of parameter as given in [40, Table I]. The suitability of the previous relations in different propagation environments have been examined through measurement data, such as wearable off-body communication (i.e., for car parking LOS environment where  $m_s$  is having the value 100 for both fading

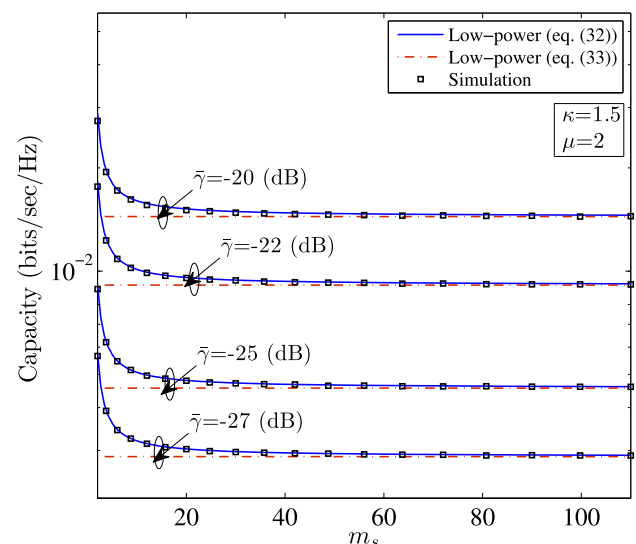


Fig. 1 ORA capacity versus  $m_s$  under low-power regime

models [40, Table II]), device-to-device (D2D) communication (i.e., for indoor non-LOS environment where  $m_s=50$  for EMIG fading model [40, Table IV]), and vehicle-to-vehicle (V2V) communication (i.e. for LOS environment where  $m_s=100$  for aforementioned composite fading models [40, Table V]).

### 5.2 Channel inversion with fixed rate

More power is given to the channel which having low SNR and vice versa. By following this approach the received power can be made constant. In other words we can say that power given by the transmitter is inversely proportional to the SNR of the fading channel. In this case fading channel is assumed as the time-invariant AWGN channel by the Tx and Rx, which further helps in reducing the dependency on the behaviour of fading channel [6, 28].

The channel capacity with CIFR adaptation scheme is defined as [26, Eq. (17)]

$$C_{CIFR} = W \log_2 \left[ 1 + \underbrace{\frac{1}{E[Y^{-1}]}}_{I_0} \right] \tag{54}$$

#### 5.2.1 CIFR for KMIG fading model

Solution of  $I_0$  in (54) is obtained by putting  $n = -1$  in [40, Eq. (8)]

$$I_0 = \left[ \frac{\mu(1 + \kappa)}{m_s \bar{\gamma}} \right] \frac{\exp(-\mu\kappa)}{B(m_s, \mu)} B(1 + m_s, \mu - 1) {}_1F_1(\mu - 1, \mu, \mu\kappa) \tag{55}$$

After incorporating the value of  $I_0$  from (55) into (54) and with some basic mathematics yields

$$C_{CIFR} = W \log_2 \left[ 1 + \frac{m_s \bar{\gamma} B(m_s, \mu) \exp(\mu\kappa)}{\mu(\kappa + 1) B(m_s + 1, \mu - 1) {}_1F_1(\mu - 1, \mu, \mu\kappa)} \right] \tag{56}$$

with the use of identity,  $\exp(-x) {}_1F_1(\hat{a}; \hat{b}; x) = {}_1F_1(\hat{b} - \hat{a}; \hat{a}; -x)$  [51, Eq. (07.20.17.0013.01)] and basic definition of beta function i.e.  $B(a, b) = \frac{\Gamma(a)\Gamma(b)}{\Gamma(a+b)}$  [50], the Eq. (56) can be written as

$$C_{CIFR} = W \log_2 \left[ 1 + \frac{\bar{\gamma}(\mu - 1)}{\mu(\kappa + 1) {}_1F_1(1; \mu; -\mu\kappa)} \right] \tag{57}$$

The expression (57) can be re-written for high values of received SNR with some basic mathematical approximation as given below

$$C_{CIFR}^{HP} = W \log_2 \left[ \frac{\bar{\gamma}(\mu - 1)}{\mu(\kappa + 1) {}_1F_1(1; \mu; -\mu\kappa)} \right] \tag{58}$$

Similarly, at low SNR, the CIFR capacity can be written in closed-form with basic mathematical approximations

$$C_{CIFR}^{LP} = \frac{W \bar{\gamma}(\mu - 1) \log_2(e)}{\mu(\kappa + 1) {}_1F_1(1; \mu; -\mu\kappa)} \tag{59}$$

For  $\mu \gg 1$ , (57), (58), and (59) can be simplified as

$$C_{CIFR} \approx W \log_2 \left[ 1 + \frac{\bar{\gamma}}{(\kappa + 1) {}_1F_1(1; \mu; -\mu\kappa)} \right] \tag{60}$$

$$C_{CIFR}^{HP} \approx W \log_2 \left[ \frac{\bar{\gamma}}{(\kappa + 1) {}_1F_1(1; \mu; -\mu\kappa)} \right] \tag{61}$$

$$C_{CIFR}^{LP} \approx \frac{W \bar{\gamma} \log_2(e)}{(\kappa + 1) {}_1F_1(1; \mu; -\mu\kappa)} \tag{62}$$

The above results are derived under the case when  $\mu \gg 1$  (i.e., number of multipath clusters are very high) which is often seen in dense urban environment where multipath components are dominant. It is observed from the Fig. 2(a–c) that the approximate results given by (60), (61), and (62) converge to (57), (58), and (59) at higher values of multipath parameter  $\mu$ .

#### 5.2.2 CIFR for EMIG fading model

Substituting  $n=-1$  into [40, Eq. (19)] and using basic definition of Beta and Gamma function [50], the solution to  $I_0$  for EMIG distribution is obtained as

$$I_0 = \frac{2\mu h}{(2\mu - 1) \bar{\gamma} h^\mu} {}_2F_1 \left( \mu - \frac{1}{2}, \mu; \mu + \frac{1}{2}; \frac{H^2}{h^2} \right) \tag{63}$$

Further, putting (63) into (54), it follows that

$$C_{CIFR} = W \log_2 \left[ 1 + \frac{(1 - \frac{1}{2\mu}) \bar{\gamma} h^{\mu-1}}{{}_2F_1(\mu - \frac{1}{2}, \mu; \mu + \frac{1}{2}; \frac{H^2}{h^2})} \right] \tag{64}$$

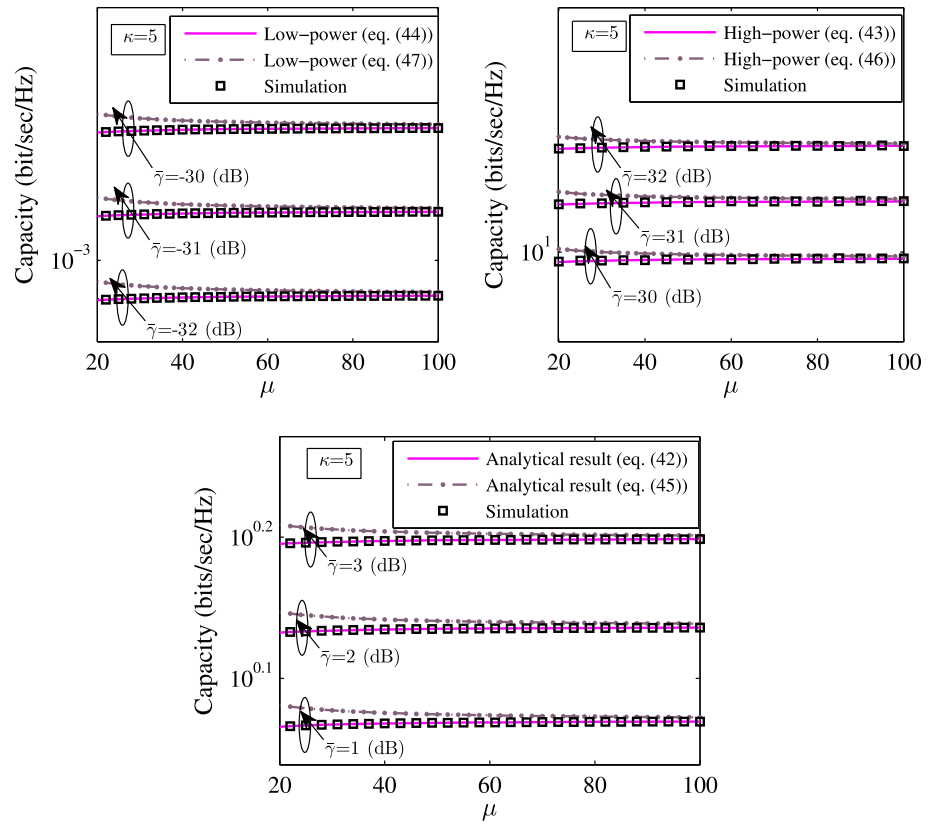
Furthermore, CIFR under EMIG composite fading model at high and low SNR can be calculated with the similar approach as in Sect. 5.2.1 which results in the following expressions

$$C_{CIFR}^{HP} \approx \log_2 \left[ \frac{(1 - \frac{1}{2\mu}) \bar{\gamma} h^{\mu-1}}{{}_2F_1(\mu - \frac{1}{2}, \mu; \mu + \frac{1}{2}; \frac{H^2}{h^2})} \right] \tag{65}$$

$$C_{CIFR}^{LP} \approx \frac{W(2\mu - 1) \bar{\gamma} \log_2(e)}{2\mu h^{1-\mu} {}_2F_1(\mu - \frac{1}{2}, \mu; \mu + \frac{1}{2}; \frac{H^2}{h^2})} \tag{66}$$

The closed-form expressions obtained in (57), (58), (59), (64), (65), and (66) do not contain shadowing parameter  $m_s$ , thus CIFR policy is independent of shadowing.

**Fig. 2** CIFR capacity versus multipath parameter  $\mu$



**5.3 Truncated CIFR**

A large amount of transmitted power is consumed in the case of CIFR for recouping the critical fading in the wireless channel. TIFR is the improved version of CIFR scheme, such that it regresses the fading only above a cut-off fading threshold ( $\gamma_0$ ) [60]. The solution of the outage capacity is given as [26, Eq. (26)]

$$C_{out} = W \log_2 \left[ 1 + \frac{1}{\int_{\gamma_0}^{\infty} \frac{f_Y(\gamma)}{\gamma} d\gamma} \right] (1 - P_{out}(\gamma_0)) \tag{67}$$

**5.3.1 TIFR for KMIG fading model**

By using (2) into integral part of (67) and employing the identity [50, Eq. (3.194.2)], the integral is simplified as

$$\begin{aligned} \int_{\gamma_0}^{\infty} \frac{f_Y(\gamma)}{\gamma} d\gamma &= \zeta \\ &= \sum_{r=0}^{\infty} \frac{(m_s + \mu)_r (\mu\kappa)^r \exp(-\mu\kappa)}{r! (\mu)_r B(m_s, \mu) (m_s + 1) (\gamma_0)^{m_s+1}} \left( \frac{m_s \bar{\gamma}}{\mu(\kappa + 1)} \right)^{m_s} \\ &\quad \times {}_2F_1 \left( \mu + r + m_s, 1 + m_s; 2 + m_s; \frac{-m_s \bar{\gamma}}{\gamma_0 \mu (\kappa + 1)} \right) \end{aligned} \tag{68}$$

Now, substituting the value of (68) into (67) and with some mathematical manipulations, reduced expression for outage capacity is given as follows

$$C_{out} = W \log_2 \left[ 1 + \frac{1}{\zeta} \right] (1 - P_{out}(\gamma_0)) \tag{69}$$

where  $P_{out}$  is the outage probability of KMIG as given in [40, Eq. 5].

The TIFR capacity expression for KMIG fading channel is derived by considering the maximum value of outage capacity over range of  $\gamma_0$

$$C_{TIFR} = \max_{\gamma_0} C_{out} \tag{70}$$

The high and low SNR solution for the outage capacity are obtained by basic mathematical approximation in (69). After following the same method as in the Sect. 5.2.1, results into

$$C_{out}^{HP} \approx -W \log_2(\xi)(1 - P_{out}(\gamma_0)) \tag{71}$$

$$C_{out}^{LP} \approx \left(\frac{1}{\xi}\right) \log_2(e)(1 - P_{out}(\gamma_0)) \tag{72}$$

### 5.3.2 TIFR for EMIG fading model

By substituting (4) into (67), and with the help of similar methodology as given in the previous Sect. 5.3.1, one can obtain the final expression for outage capacity as

$$C_{out} = W \log_2 \left[ 1 + \frac{1}{\chi} \right] (1 - P_{out}(\gamma_0)) \tag{73}$$

where  $P_{out}$  is given by [40, Eq. 14] and  $\chi$  is defined as follows

$$\chi = \sum_{r=0}^{\infty} \frac{\Gamma(\mu + r) H^{2r} {}_2F_1 \left( m_s + 2\mu + 2r, m_s + 2r + 1; m_s + 2r + 2; \frac{-m_s \bar{\gamma}}{\gamma_0 2\mu h} \right)}{\Gamma(\mu) r! B(m_s, 2\mu + 2r) (m_s + 2r + 1) h^{\mu+2r} (2\mu h)^{m_s} (m_s \bar{\gamma})^{-m_s}} \tag{74}$$

The TIFR capacity expression for EMIG fading channel is derived by considering the maximum value of outage capacity over range of  $\gamma_0$  as given in (70). The high and low SNR solution for the outage capacity are obtained with the use of simple mathematical approximations in (73), with following the methodology stated in Sect. 5.2.1.

## 6 Results and discussion

In this section, the proposed analytical formulations of KMIG and EMIG composite fading channels are validated through numerical and simulated results. In addition, we present multiple plots of various performance matrices to visualize the impact of fading parameters. It is noted from the plots that Monte-Carlo simulation (generated by considering  $10^6$  number of random variables) and proposed analytical results perfectly coincide for wide range of the

considered system parameters. It is also observed that the derived expressions are containing simplified mathematical functions which are directly available in MATLAB. For the simulation of the provided analytical results (expressions with infinite summation), we have considered 25 number of summation terms such that the relative error of  $10^{-6}$  is achieved.

The average SEP of KMIG and EMIG composite fading channels for different fading scenarios are depicted in Figs. 3 and 4. In Fig. 3, the average SEP of KMIG composite fading model is demonstrated for  $M$ -ary phase shift keying (MPSK) with constellation size  $M = 8, 16,$  and  $32$ . The figure shows the exact result obtained by numerically solving (7), the analytical result (8), and the Monte-Carlo simulation are in perfect agreement. The asymptotic results obtained in (32) are also included in this figure. The fading parameters, such as  $\kappa = 1.2, \mu = 2,$  and  $m_s = 4$  are considered. It is clearly evident from the figure that average SEP degrades with constellation size which supports the theoretical concepts, as constellation size increases, the Euclidean distance between symbols decreases which further results in a higher probability of error. It is clearly visible that the asymptotic plots are in perfect agreement with the simulation results. Performance of the EMIG

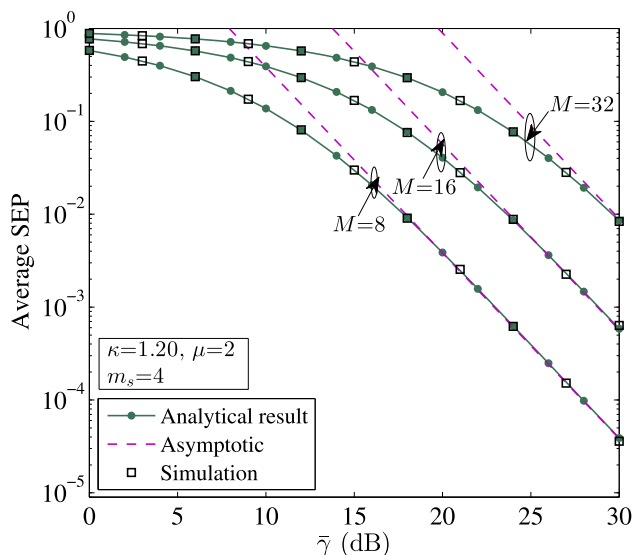
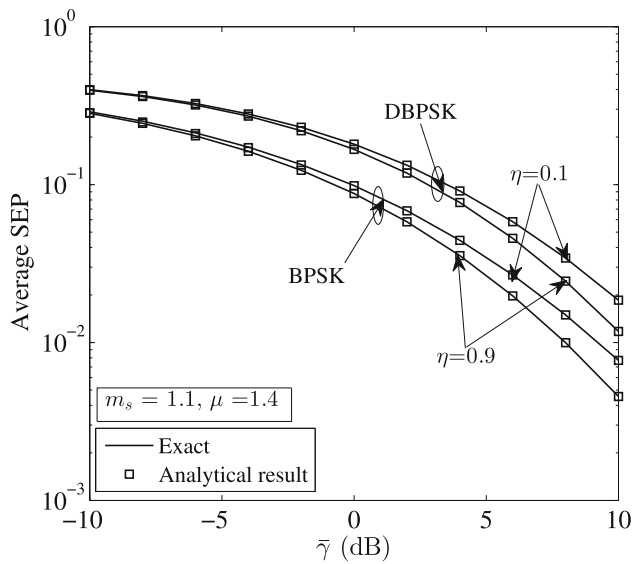
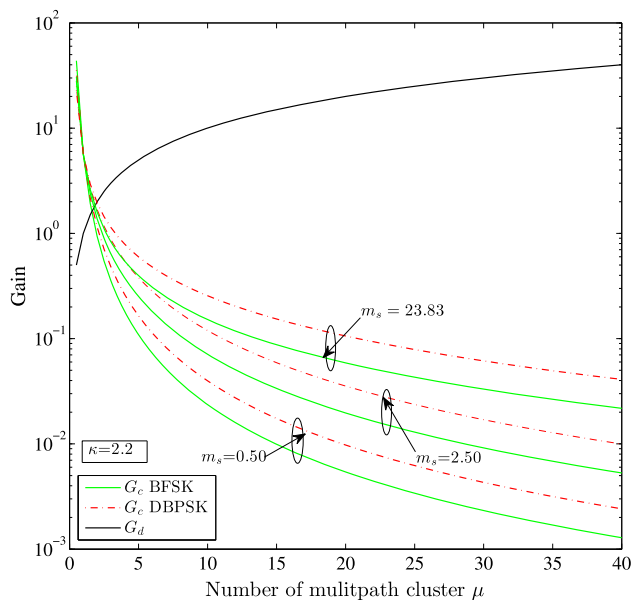


Fig. 3 Average SEP of KMIG composite fading channel for MPSK with different constellation sizes

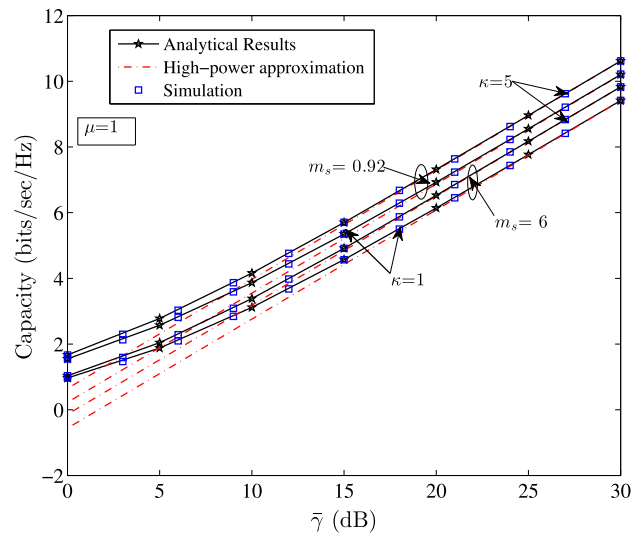


**Fig. 4** Average SEP of EMIG composite fading channel for BPSK and DBPSK with different values of fading parameters ( $\mu = 1.4$ ,  $m_s = 1.1$  and  $\eta = 0.1$  &  $0.9$ )

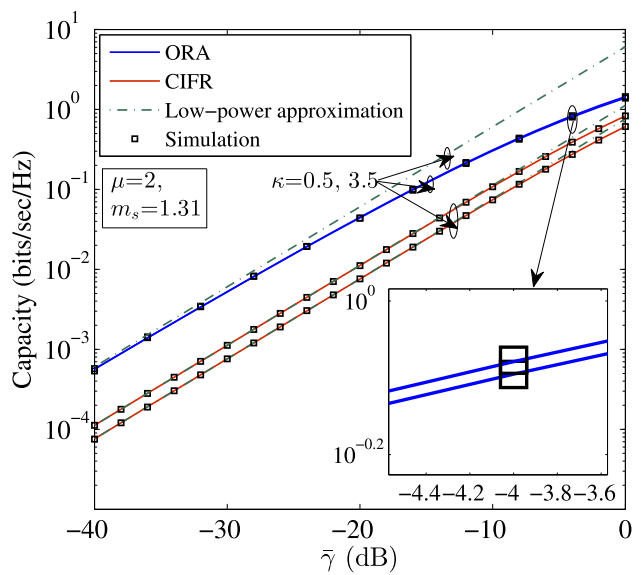


**Fig. 5** Coding and diversity gain as a function of number of multipath clusters

composite fading channel is evaluated under coherent binary phase shift keying (BPSK) and non-coherent differential binary phase shift keying (DBPSK) modulation scheme with  $m_s = 1.1$  and  $\mu = 1.4$  in Fig. 4. It is clearly visible that the numerical solutions are in agreement with the analytical results obtained through (13) and (21). As we know that coherent modulation schemes are superior to non-coherent modulation schemes and similar observation has been made from the figure. It is perceived from the



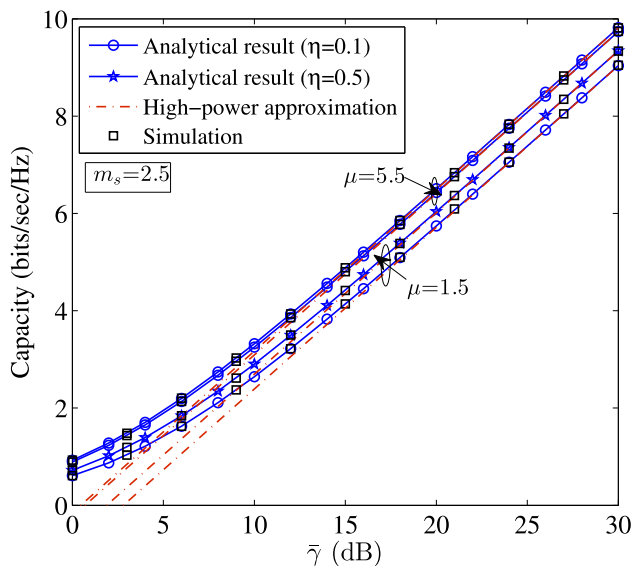
**Fig. 6** Channel capacity of KMIG composite fading channel under ORA scheme with  $\kappa = 1, 5$  and  $m_s = 0.92, 6$



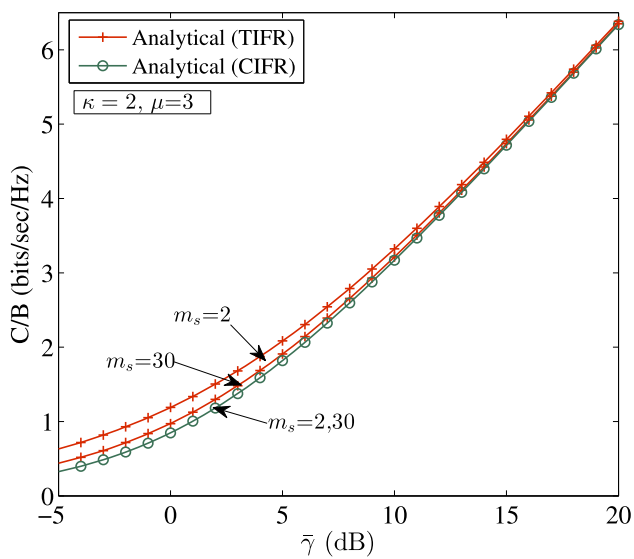
**Fig. 7** Channel capacity of KMIG composite fading channel under ORA and CIFR with low SNR approximations

figure that the channel conditions improve with the  $\eta$  (0.1 to 0.9), as the average SEP plot shows a downward shift.

In Fig. 5, coding and diversity gain are given as a function of number of multipath clusters ( $\mu$ ). It is visible from the plot that, the coding gain decreases gradually with the parameter  $\mu$  while the diversity gain improves. This also validate the previously obtained expression of the diversity gain as it is directly proportional to the parameter  $\mu$ . On the other hand coding gain is dependent on all other fading parameters ( $\kappa$ ,  $\mu$  and  $m_s$ ) as clear from the figure as well as from the numerical expressions. Superiority of



**Fig. 8** Channel capacity of EMIG composite fading channel under CIFR scheme with  $\eta = 0.1, 0.5, m_s = 2.5$  and  $\mu = 1.5, 5.5$



**Fig. 9** Channel capacity under CIFR and TIFR schemes for KMIG composite fading channel with  $m_s = 2, 30, \kappa = 2$  and  $\mu = 3$

coherent modulation schemes over non-coherent is also validated from this figure which supports the theoretical concept.

Figures 6, 7, 8, 9 deal with the channel capacity analysis of KMIG and EMIG composite fading channels under different adaptation schemes. Figure 6 indicates the effect of fading on the channel capacity under ORA scheme over KMIG composite distribution. The analytical solutions are plotted with the help of (43) and validated with Monte Carlo simulations. The analysis of the results is done at the

single value of  $\mu$  and different values of  $\kappa$  and  $m_s$ . It is clearly detectable from the figure that channel capacity enhances by decreasing the value of  $m_s$  and increasing the values of  $\kappa$  from 1 to 5, satisfying the theoretical concepts. Furthermore, the high SNR approximation result (45) is included in this figure. The result perfectly coincides to the analytical result at high-power. Low SNR approximation of ORA (47) and CIFR (59) adaptation schemes are compared under different fading conditions over the KMIG composite fading model in Fig. 7. It is clearly evident from the plot that CIFR scheme has significant variation by increasing the value of shadowing parameter  $\kappa$  from 0.5 to 3.5 while no such variation is noticed in the case of ORA. It is also observed that low-power ORA analysis is independent of fading parameter  $\kappa$ .

Figure 8 depicts the analytical result of CIFR capacity for EMIG composite fading model obtained through (64) at different values of multipath parameters, i.e.  $\eta$  and  $\mu$  while shadowing parameter  $m_s$  is kept constant. An increase in the values of  $\eta$  and  $\mu$  must ensure the improvement in channel capacity, and it is perceived from the figure that increase in the values of  $\eta$  (0.1 to 0.5) and  $\mu$  (1.5 to 5.5), the capacity curve under CIFR shifts upwards. High SNR approximations with the help of derived analytical result of (58) are also shown in the figure. It is inferred from the figure that as the channel condition becomes more severe, the high-power solution converges toward much higher values of SNR, which in turn is supported from the observations noticed in the Fig. 6.

Channel capacity under CIFR and TIFR for KMIG composite fading model is compared in Fig. 9 with different values of shadowing parameter  $m_s$ . It is a well-known fact that the TIFR is superior to CIFR adaptation scheme, and similar observation is evident from the figure for same values of fading parameters, satisfying the theoretical concepts. It is also clear from the figure that increasing the value of shadowing parameter  $m_s$  from 2 to 30 shows a significant impact on TIFR schemes, whereas in the case of CIFR no such impact is visible (as can be verified from the derived result 57 that is independent of shadowing parameters). On the other hand, it is noted that CIFR converges to TIFR at high SNR showing a similar impact on the capacity of the system.

### 7 Conclusion

In this paper, the performance analysis of wireless channels over composite KMIG and EMIG fading models has been carried out. First, the novel analytical expressions for average SEP under coherent and non-coherent modulation schemes, such as MPSK, BPSK, DBPSK, etc., was developed for the KMIG and EMIG composite fading

models. Moreover, the effect of fading parameters on channel conditions were demonstrated with the help of asymptotic solutions with coding and diversity gain. A comparative analysis among various adaptation schemes of the channel capacity, such as ORA, CIFR, and TIFR has been carried out. While considering practical cases approximate results are obtained for ORA (under low-power regime) and CIFR (specifically for KMIG model). The significant effect of composite fading conditions on the performance of wireless channels has been identified for different values of SNR. All the results have been compared with Monte-Carlo simulations and with the exact results to authenticate the correctness of the proposed analytical solutions. Finally, the results of the current paper are of significant importance as these solutions can be utilized in the investigation of the traditional as well as modern wireless systems.

## References

- Dong, Y., & Fan, P. (2013). Bounds on the average transmission rate in high speed railway wireless communications. *International Workshop on High Mobility Wireless Communications (HMWC), Shanghai* (pp. 142–145).
- Nezami, Z., & Zamanifar, K. (2019). Internet of things/Internet of everything: Structure and ingredients. *IEEE Potentials*, 38(2), 12–17.
- Costanzo, A., & Masotti, D. (2017). Energizing 5G: Near-and far-field wireless energy and data transfer as an enabling technology for the 5G IoT. *IEEE Microwave Magazine*, 18(3), 125–136.
- Ma, Z., Xiao, M., Xiao, Y., Pang, Z., Poor, H. V., & Vucetic, B. (2019). High-reliability and low-latency wireless communication for internet of things: Challenges, fundamentals, and enabling technologies. *IEEE Internet of Things Journal*, 6(5), 7946–7970.
- Yoo, S. K., Cotton, S. L., Sofotasios, P. C., Matthaiou, M., Valkama, M., & Karagiannidis, G. K. (2017). The Fisher–Snedecor F distribution: A simple and accurate composite fading model. *IEEE Communication Letters*, 21(7), 1661–1664.
- Pant, D., Chauhan, P. S., & Soni, S. K. (2019). Error probability and channel capacity analysis of wireless system over inverse gamma shadowed fading channel with selection diversity. *International Journal of Communication Systems*, 32(16), e4083.
- Chauhan, P. S., Rana, V., Kumar, S., Soni, S. K., & Pant, D. (2019). Performance analysis of wireless communication system over non-identical cascaded generalised gamma fading channels. *International Journal of Communication Systems*, 32(13), e4004.
- Bhargav, N., Cotton, S. L., & Simmons, D. E. (2016). Secrecy capacity analysis over  $\kappa - \mu$  fading channels: Theory and applications. *IEEE Transactions on Communications*, 64(7), 3011–3024.
- Ramírez-Espinosa, P., & Lopez-Martinez, F. J. (2019). On the Utility of the inverse gamma distribution in modeling composite fading channels. arXiv preprint arXiv: [arXiv:1905.00069v1](https://arxiv.org/abs/1905.00069v1).
- Yoo, S. K., Cotton, S. L., Sofotasios, P. C., & Freear, S. (2016). Shadowed fading in indoor off-body communications channels: A statistical characterization using the  $\kappa - \mu$ /gamma composite fading model. *IEEE Transactions on Wireless Communications*, 15(8), 5231–5244.
- Bithas, P. S. (2009). Weibull-gamma composite distribution: Alternative multipath/shadowing fading model. *IET Electronics Letters*, 45(14), 749–751.
- Laourine, A., Alouini, M. S., Affes, S., & Stephenne, A. (2009). On the performance analysis of composite multipath/shadowing channels using the G-distribution. *IEEE Transactions on Communications*, 57(4), 1162–1170.
- Singh, R., Rawat, M., & Pradhan, P. M. (2020). Effective capacity of wireless networks over double shadowed Rician fading channels. *Wireless Networks*, 26, 1347–1355.
- Yoo, S. K., Cotton, S. L., Sofotasios, P. C., Matthaiou, M., Valkama, M., & Karagiannidis, G. K. (2015). The  $\kappa - \mu$  inverse gamma fading model. In *IEEE 26th Annual international symposium on personal, indoor, and mobile radio communications (PIMRC), Hong Kong* (pp. 425–429).
- Yoo, S. K., Sofotasios, P. C., Cotton, S. L., Matthaiou, M., Valkama, M., & Karagiannidis, G. K. (2015). The  $\eta - \mu$  inverse gamma composite fading model. In *IEEE 26th annual international symposium on personal, indoor, and mobile radio communications (PIMRC), Hong Kong* (pp. 166–170).
- Sofotasios, P. C., Theodoros, A. T., Ghogho, M., Wilhelmsson, L. R., & Valkama, M. (2013). The  $\eta - \mu$ /IG distribution: A novel physical multipath/shadowing fading model. In *IEEE ICC 2013-wireless communications symposium* (pp. 5715–5719).
- Yacoub, M. D. (2007). The  $\kappa - \mu$  Distribution and  $\eta - \mu$  distribution. *IEEE Antennas and Propagation Magazine*, 49(1), 68–81.
- Garca-Corales, C., Canete, F. J., & Paris, J. F. (2014). Capacity of  $\kappa - \mu$ / shadowed fading channels. *HINDAWI International Journal of Antennas and Propagation* (pp. 1–8).
- Yacoub, M. D. (2007). The  $\alpha - \mu$  distribution: A physical fading model for the Stacy distribution. *IEEE Transactions on Vehicular Technology*, 56(1), 27–34.
- Heliot, F., Ghavami, M., & Nakhai, M. R. (2008). An accurate closed-form approximation of the average probability of error over log-normal fading channel. *IEEE Transactions on Wireless Communications*, 7, 1495–1500.
- Pan, G., Ekici, E., & Feng, Q. (2012). Capacity analysis of log-normal channel under various adaptive transmission schemes. *IEEE Communication Letters*, 16, 346–348.
- Enserink, S., & Fitz, P. M. (2013). Estimation of constrained capacity and outage probability in lognormal channels. *IEEE Transactions on Vehicular Technology*, 62, 399–404.
- Khandelwal, V., & Karmeshu., (2015). Channel capacity analysis over slow fading environment: Unified truncated moment generating function approach. *Wireless Personal Communications*, 82, 2377–2390.
- Safak, A. (1993). Statistical analysis of the power sum of multiple correlated log-normal components. *IEEE Transactions on Vehicular Technology*, 42, 58–61.
- Sakarellos, V. K., Skraparlis, D., Panagopoulos, A. D., & Kanellopoulos, J. D. (2008). Performance of MRC satellite diversity receivers over correlated log-normal and gamma fading channels. *10th international workshop on signal processing for space communication (SPSC)*.
- Tiwari, D., Soni, S. K., & Chauhan, P. S. (2017). A new closed-form expressions of channel capacity with MRC, EGC and SC over lognormal fading channels. *Wireless Personal Communications*, 97, 4183–4197.
- Chauhan, P. S., & Soni, S. K. (2018). New analytical expressions for ASEP of modulation techniques with diversity over log-normal fading channels with application to interference-limited environment. *Wireless Personal Communications*, 99, 695–716.
- Rana, V., Chauhan, P. S., Soni, S. K., & Bhatt, M. (2017). A new closed-form of ASEP and Channel capacity with MRC and selection combining over Inverse Gaussian shadowing.

- International Journal of Electronics and Communications (AEU)*, 74, 107–115.
29. Ram'irez-Espinosa, P., & L'opez-Mart'inez, F. J. (2020). Composite fading models based on inverse gamma shadowing: Theory and validation. [arXiv:1905.00069v3](https://arxiv.org/abs/1905.00069v3).
  30. Pant, D., Chauhan, P. S., Soni, S. K., & Naithani, S. (2020). Channel capacity analysis of wireless system under ORA scheme over  $\kappa - \mu$  inverse gamma and  $\eta - \mu$  inverse gamma composite fading models. In *2020 international conference on electrical and electronics engineering (ICE3), Gorakhpur, India* (pp. 425–430).
  31. Alam, S., & Annamalai, A. (2012). Energy detector's performance analysis over the wireless channels with composite multipath fading and shadowing effects using the AUC approach. In *2012 IEEE consumer communications and networking conference*, vol. 74 (pp. 771–775).
  32. Shanker, P. M. (2004). Error rates in generalized shadowed fading channels. *Wireless Personal Communications*, 28, 233–238.
  33. Abdi, A., & Kaveh, M. (2009). Weibull-gamma composite distribution: Alternative multipath/shadowing fading model. *Electronics Letters*, 45(14), 749–751.
  34. Sofotasios, P. C., & Freear, S. (2011). On the  $\kappa - \mu$ /Gamma composite distribution: A generalized multipath/shadowing fading model. *Proceedings IEEE ICOM*, 45, 390–394.
  35. Zhang, J., Matthaiou, M., Tan, Z., & Wang, H. (2012). Performance analysis of digital communication systems over composite  $\eta - \mu$ /Gamma fading channels. *IEEE Transactions on Vehicular Technology*, 61(7), 3114–3124.
  36. Yoo, S. K., Cotton, S. L., Sofotasios, P. C., & Freear, S. (2011). Shadowed fading in indoor off-body communication channels: A statistical characterization using the  $\kappa - \mu$ /Gamma composite fading model. *IEEE Transactions on Wireless Communications*, 5(8), 5231–5244.
  37. Al-Hmood, H., & Al-Raweshidy, H. S. (2017). Unified modelling of composite  $\kappa - \mu$ /Gamma,  $\eta - \mu$ /Gamma, and  $\alpha - \mu$ /Gamma fading channels using a mixture Gamma distribution with application to energy detection. *IEEE Antennas Wireless Propagation Letters*, 16, 104–108.
  38. Al-Ahmadi, S., & Yanikomeroğlu, H. (2010). On the approximation of the generalized-distribution by a gamma distribution for modeling composite fading channels. *IEEE Transactions on Wireless Communications*, 9(2), 706–713.
  39. Karmeshu and Agrawal R., (2007). On efficacy of Rayleigh-inverse Gaussian distribution over  $K$ -distribution for wireless fading channels. *Wireless Communication and Mobile Computing*, 7, 1–7.
  40. Yoo, S. K., Bhargav, N., & Cotton, S. L., et al. (2017). The  $\kappa - \mu$ /Inverse Gamma and  $\eta - \mu$ /Inverse Gamma composite fading models: fundamental statistics and empirical validation. *IEEE Transaction on Communications*.
  41. Sofotasios, P. C. et al. (2018). Capacity analysis under generalized composite fading conditions. In *International conference on advanced communication technologies and networking (CommNet)*, Marrakech (pp. 1–10).
  42. Glen, A. G. (2017). On the inverse gamma as a survival distribution. In *Computational probability applications* (pp. 15–30).
  43. Badarneh, O. S. (2020). The  $\alpha$ - $\eta$ - $\mathcal{F}$  and  $\alpha$ - $\kappa$ - $\mathcal{F}$  composite fading distributions. *IEEE Communications Letters*, 24(9), 1924–1928.
  44. Yoo, S. K., Sofotasios, P. C., Cotton, S. L., Muhaidat, S., Lopez-Martinez, F. J., Romero-Jerez, J. M., & Karagiannidis, G. K. (2020). A comprehensive analysis of the achievable channel capacity in  $\mathcal{F}$  composite fading channels. *IEEE Access*, vol. 7 (pp. 34078–34094).
  45. Badarneh, O. S., Shawaqfeh, M. K., & Kadoch, M. (2020). Performance analysis of mobile IoT networks over composite fading channels. In *International wireless communications and mobile computing (IWCMC)* (pp. 1234–1239).
  46. Rabie, K., Makarfi, A. U., Kharel, R., Badarneh, O. S., Adebisi, B., Li, X., & Ding, Z. (2020). On the Performance of non-orthogonal multiple access over composite fading channels. [arXiv: 2004.07860v1](https://arxiv.org/abs/2004.07860v1).
  47. Bithas, P. S., Nikolaidis, V., Kanatas, A. G., & Karagiannidis, G. K. (2020). UAV-to-ground communications: Channel modeling and UAV selection. *IEEE Transactions on Communications*, 68(8), 5135–5144.
  48. Sofotasios, P. C., et al. (2018). Ergodic capacity analysis of wireless transmission over generalized multipath/shadowing channels. In *2018 IEEE 87th vehicular technology conference (VTC Spring), Porto* (pp. 1–5).
  49. Sofotasios, P. C., et al. (2018). Error analysis of wireless transmission over generalized multipath/shadowing channels. In *2018 IEEE wireless communications and networking conference (WCNC), Barcelona* (pp. 1–6).
  50. Gradshteyn I. S., & Ryzhik I. M. (2007). Table of integrals, series, and products, 7th edn. Academic Press, New York.
  51. Wolfram Research, Inc. (2019). visited on 01/12/2019. <http://functions.wolfram.com/id>.
  52. Badarneh, O. S., & Aloqlah, M. S. (2016). Performance analysis of digital communication systems over  $\alpha - \eta - \mu$  fading channels. *IEEE Transaction on Vehicular Technology*, 65(10), 7972–7981.
  53. Prudnikov, A. P., Brychkov, Y. A., & Marichev, O. I. (1986). Integral series, Elementary functions. The Netherlands: Gordon and Breach (p. 2).
  54. Srivastava, H. M., Rahman, G., & Nisar, K. S. (2019). Some extensions of the pochhammer symbol and the associated hypergeometric functions. *Iranian Journal of Science and Technology, Transactions A: Science*, 43, 2601–2606.
  55. Prudnikov, A. P., Brychkov, Y. A., & Marichev, O. I. (1986). *Integral series*. Elementary functions, The Netherlands: Gordon and Breach (p. 1).
  56. Chauhan, P. S., Tiwari, D., & Soni, S. K. (2017). New analytical expressions for the performance metrics of wireless communication system over Weibull/Lognormal composite fading. *International Journal of Electronics and Communication (AEU)*, 82, 397–405.
  57. Simon, M. K., & Alouini, M. S. (1998). A unified approach to the probability of error for noncoherent and differentially coherent modulations over Generalized fading channels. *IEEE Transaction on Communication*, 46(12), 1625–1638.
  58. Chauhan, P. S., & Soni, S. K. (2019). Average SEP and channel capacity analysis over Generic/IG composite fading channels: A unified approach. *Physical Communication*, 34, 9–18.
  59. Chauhan, P. S., Kumar, S., & Soni, S. K. (2019). New approximate expressions of average symbol error probability, probability of detection and AUC with MRC over generic and composite fading channels. *International Journal of Electron. and Communication (AEU)*, 99, 119–129.
  60. Marvin, K. S., & Alouini, M. S. (2000). *Digital communication over fading channels*. Hoboken, New Jersey: John Wiley and Sons Inc.



61. Wang, Z., & Giannakis, G. B. (2003). A simple and general parametrization quantifying performance in fading channels. *IEEE Transactions on Communications*, 51(8), 1389–1398.

**Publisher's Note** Springer Nature remains neutral with regard to jurisdictional claims in published maps and institutional affiliations.



**Diwaker Pant** was born in Pauri Garhwal, India. He received his B.Tech. degree in Electronics and Communication Engineering from Kurukshetra University Kurukshetra, India in 2008, and the M.E. degree in Electronics and Communication Engineering from National Institute of Technical Teachers Training and Research (NITTTR) Chandigarh, India in 2013, and is currently working toward the Ph.D. degree at Uttarakhand Technical University, Dehradun, India. He is an eminent academician having more than 10 years of teaching experience. Currently he is working with Tula's Institute (Uttarakhand Technical University), Dehradun as Assistant Professor in Electronics and Communication Engineering Department. He has published more than 15 scientific research publications in reputed International Journals and Conferences. His research Interest includes the Wireless Communication, Propagation Channel Modeling, Embedded Systems, and Wireless Sensor Networks.



**Puspriaj Singh Chauhan** was born in UP, India. He received his Bachelor of Technology in Electronics and Communication Engineering from Uttar Pradesh Technical University, India in 2009, the M.Tech. degree in Digital Signal Processing from Govind Ballabh Pant Engineering College, Pauri, Uttarakhand, India in 2011. He has submitted his Ph.D. thesis at Uttarakhand Technical University, Uttarakhand, India in 2019. Currently, he is working under project

funded by Ministry of Electronics and Information Technology

(MeitY) at M.M.M. University of Technology, Gorakhpur, India. His research interests include Wireless Communication and Propagation Channel Modeling.



**Sanjay Kumar Soni** was born in UP, India on March 1975. He received his Bachelor of Engineering in Electronics Engineering from Madan Mohan Malviya Engineering College, Gorakhpur, Uttar Pradesh, India in 1997, the M.Tech. degree in Communication Engineering from IIT Kanpur in 2004, and Ph.D. in wireless Communication Engineering from IIT Kharagpur, India in 2011. Currently he is working as Dean Research and Consultancy in

M.M.M. University of Technology, Gorakhpur, India. His research interests include Wireless Communication, Propagation Channel Modeling, Cognitive Radio, MIMO-OFDM, UWB Communication, and Statistical Characterization of Wireless Channel.



**Sanjeev Naithani** received the B.E. degree in Electronics and Communication Engineering from G.B. Pant Engineering College, Pauri Garhwal, India in 2000, and M.Tech degree in Laser Technology from Indian Institute of Technology, Kanpur India. He has completed his master's thesis (2006–07) from TU Berlin Germany through DAAD scholarship. He completed his Ph.D. from Ghent University, Belgium in 2015. He has more than 20 Years of

teaching, research and development experience. Currently he is working as Associate Professor in Electronics and Communication Engineering Department at G.B. Pant Institute of Engineering and Technology, Pauri Garhwal, Uttarakhand, India. His research area includes Communications, Organic Electronics, and Optoelectronics.